Correspondence to:
K. M. Moore and A. Barik,
kimberly.moore@aya.yale.edu;
abarik@jhu.edu

Dynamo Simulations of Jupiter's Magnetic Field: The Role of Stable Stratification and a Dilute Core

K. M. Moore[1] , A. Barik[2] , S. Stanley[2,3] , D. J. Stevenson[1] , N. Nettelmann[4] , R. Helled[5] , T. Guillot[6] , B. Militzer[7] , and S. Bolton[8]

[1]Division of Geological & Planetary Sciences, California Institute of Technology, Pasadena, CA, USA, [2]Department of Earth & Planetary Sciences, Johns Hopkins University, Baltimore, MD, USA, [3]Applied Physics Laboratory, Johns Hopkins University, Laurel, MD, USA, [4]Institute of Planetary Research, German Aerospace Center (DLR), Berlin, Germany, [5]Institute for Computational Science, Center for Theoretical Astrophysics & Cosmology, University of Zurich, Zürich, Switzerland, [6]Université Côte d'Azur, Observatoire de la Côte d'Azur, CNRS, Laboratoire Lagrange, Nice, France, [7]Department of Earth and Planetary Science, University of California, Berkeley, CA, USA, [8]Southwest Research Institute, San Antonio, TX, USA

Abstract Understanding Jupiter's present-day interior structure and dynamics is key to constraining planetary accretion models. In particular, the extent of stable stratification (i.e., non-convective regions) in the planet strongly influences long-term cooling processes, and may record primordial heavy element gradients from early in a planet's formation. Because the Galileo entry probe measured a subsolar helium abundance, Jupiter interior models often invoke an outer stably stratified region due to helium rain. Additionally, Juno gravity data suggest a deeper, potentially stratified dilute core extending halfway through the planet. However, fits to Jupiter's gravitational data are non-unique, and outstanding uncertainty over the equations of state for hydrogen and helium remain. Here, we use high-resolution numerical magnetohydrodynamic simulations of Jupiter's magnetic field to place constraints on the extent of stable stratification within the planet. We find that compared to traditional interior models, an upper stably stratified layer between 0.9 and 0.95 Jupiter radii (R_J) helps to explain both Jupiter's dipolar magnetic field and zonal winds. In contrast, an extended dilute core that is entirely stably stratified (no convective layers) yields significantly worse fits to both. However, our models with extended deep stratification still generate dipolar magnetic fields if an upper stratified region is also present. Overall, we find that a planet with a dilute core i.e., strongly stably stratified is increasingly challenging to reconcile with Jupiter's magnetic field and winds. Thus if a dilute core is present, alternative modalities such as a fully convective dilute core, a complex multilayered interior structure, or double diffusive convection may be required.

Plain Language Summary Giant planets like Jupiter provide important clues to how the solar system formed. Jupiter is often thought of as a dynamic and well-mixed ball of hydrogen and helium gas that has been convectively cooling for billions of years. However, data from the NASA Juno Mission spacecraft suggests large regions of the planet may actually be "stably stratified," that is, not convective. Understanding the extent of this process is important since it would affect how Jupiter's temperature cools over time, and may challenge our ideas of how giant planets are formed. In this paper, we simulate the fluid dynamics of Jupiter's interior to investigate two potential stable regions: (a) an upper region (potentially due to helium rain, where helium and hydrogen separate like oil and water) and (b) a lower stratified region corresponding to the so-called "dilute core," which may extend halfway through the planet. We find that the upper stable layer helps explain both Jupiter's magnetic field and winds. In contrast, the lower stratified region does not explain either unless the upper stable layer is also present. Our results have implications for the present-day interior dynamics of giant planets, as well as their past formation and evolution.

1. Introduction

1.1. Jupiter's Interior: A Relic of Planetary Formation

The formation and evolution of our solar system remains an outstanding question in planetary science (see Helled and Morbidelli (2021) for a review). Clues to these processes, however, remain in the form of the present day interiors of our planets (Helled et al., 2022). Variations on planetary formation pathways such as core accretion (Pollack et al., 1996), pebble accretion (Johansen & Lambrechts, 2017), or disk instability; early solar system conditions, and formation location will affect many physical properties such as the planet's heavy element

distribution, and the amount of mixing that occurs over time. In this work, we will focus on the amount and extent of stably stratified (non-convective) regions in Jupiter's interior. As we discuss below, stably stratified regions play a key role in understanding some of Jupiter's largest outstanding questions, ranging from the planet's core to the atmosphere.

One significant question of interest is the structure of Jupiter's core. For simplicity, researchers typically analyze Jupiter's interior via a three-layer interior model (consisting of a small compact core of 0–20 Earth masses in the planet's center, surrounded by a liquid metallic hydrogen shell and an outer atmospheric envelope) (Gudkova & Zharkov, 1999; Guillot, 1999; Hubbard & Militzer, 2016). Since rock, ice, and iron are soluble in liquid metallic hydrogen (González-Cataldo et al., 2014; Wahl et al., 2013; Wilson & Militzer, 2011), the metallic hydrogen shell may be enriched in heavy elements, in what is known as a "dilute" core. This heavy element enrichment may be evenly mixed throughout the fluid shell, or it may be inhomogeneously distributed (Miguel et al., 2022; Nettelmann et al., 2008). Recent analysis of Juno (Jupiter) and Cassini (Saturn) gravity data (Debras & Chabrier, 2019; Guillot et al., 2018; Militzer et al., 2022; Movshovitz et al., 2020; Wahl et al., 2017) and seismology data (Mankovich & Fuller, 2021) is highly suggestive of the gas giant planets having "fuzzy," inhomogeneous dilute cores. Such cores may include heavy element gradients that extend throughout half the planet's radius, possibly strong enough to be stably stratified against convection. Still, the persistent uncertainty in the equations of state and non-uniqueness in the interpretation of gravity measurements, for example, Miguel et al. (2016), Debras and Chabrier (2019), and Miguel et al. (2022), mean that a large range of core scenarios are still possible.

The possible existence and dynamics of an inhomogenous, stratified dilute core are challenging to reconcile with traditional planetary accretion theories (Helled et al., 2022). Conceivably, a dilute core could either be a relic of formation (from initial mixing during formation or late-falling heavy elements), or due to erosion of the central core during the planet's subsequent 4 billion years of evolution. However, formation and evolution models show that either there is not enough initial energy to start dissolving the core at all, or there is too much energy and the heavy element gradients are fully erased within a few million years of formation (Müller et al., 2020). Explaining the contrast between in situ planetary formation models and present-day gravity analysis may require turning to alternative scenarios such as a giant impact (Liu et al., 2019) after Jupiter has cooled substantially, or migration from a colder, heavy-element rich location at 10+ AU (Shibata & Helled, 2022). If a dilute core is indeed present, the exact density gradients within it would provide key constraints on Jupiter's primordial accretion and subsequent evolution. Thus, finding additional methods to constrain the density gradients within Jupiter's interior is essential to understanding the formation of our solar system.

In addition to the implications for Jupiter's core, the physics of hydrogen and helium at high pressures may lead to additional regions of stable stratification within Jupiter. Specifically, as hydrogen transitions to a liquid metal near the surface of the planet ($\sim$0.85–0.9 R_J, where 1 R_J is Jupiter's radius), helium may become briefly insoluble and rain out of solution (Stevenson & Salpeter, 1977). Physically, the heavier helium droplets sink inwards (releasing gravitational energy), leaving behind a lighter layer of helium-depleted hydrogen. Depending upon the amount of depletion, stably stratified region could develop, which would inhibit heat transfer from the deeper interior. However, there is significant disagreement regarding the phase diagram of H/He immiscibility (Brygoo et al., 2021; Fortney & Hubbard, 2003; Lorenzen et al., 2011; Morales et al., 2013; Schöttler & Redmer, 2018; Stevenson & Salpeter, 1977), though these predictions broadly suggest it would occur at 1 Mbar or deeper, that is, <0.86 RJ (Hubbard & Militzer, 2016; Mankovich & Fortney, 2020; Nettelmann et al., 2015) (see Figure 1). Still, the uncertainties in the H/He phase diagram map onto a wide range of predictions for the onset timing and extent of helium rainout (Mankovich & Fortney, 2020). Searching for and constraining the extent of stratification inside of Jupiter is thus critical to modeling the planet's evolution—and ultimately, the processes driving its original formation.

Finally, Juno gravity data has highlighted one last major puzzle for stratification within Jupiter. While it has long been known that interior models require atmospheric heavy element abundances that are lower than protosolar values unless ad hoc changes to the H/He equation of state are introduced (Hubbard & Militzer, 2016), this issue has become particularly apparent with the increasing precision of the Juno gravity data and their coupling to wind models. Perturbations of the H/He-adiabat (Nettelmann et al., 2021; Wahl et al., 2017), superadiabatic or double diffusive regions (Debras & Chabrier, 2019), or artificially increased surface temperatures (Miguel et al., 2022; Nettelmann et al., 2021) have been invoked. Those models commonly suggest that the outermost
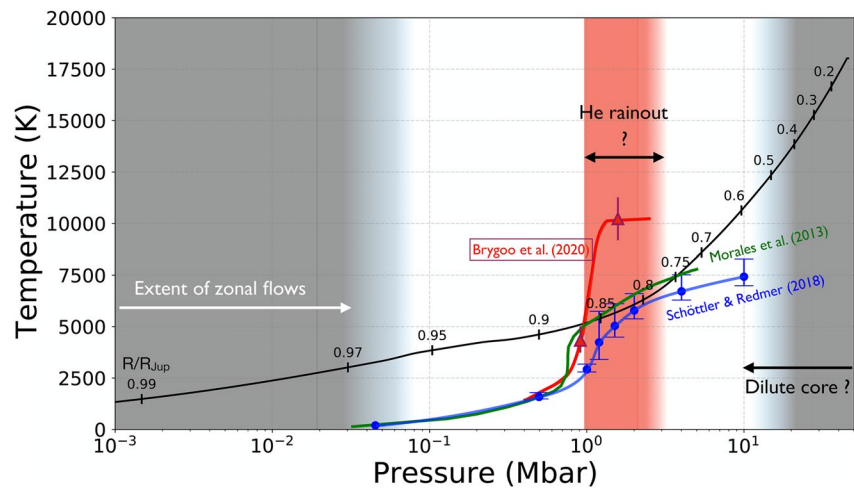
Figure 1. *Predictions of helium de-mixing from H/He equations of state.* We show the immiscibility curve of several literature models (Morales et al. (2009): green line, Schöttler and Redmer (2018): blue line, and Brygoo et al. (2021): red line) along with the associated data points and uncertainty bars, as well as a Jovian pressure-temperature curve (numbered black line). For all models, H/He immiscibility begins at approximately 1 MBar or deeper (shaded region).

region of Jupiter is not simply adiabatic and convective. Independently Christensen et al. (2020), suggest the presence of a convectively stable shell around 0.95–0.97 R_J in order to explain the attenuation of the zonal wind speeds there. However, this stable region is located shallower (closer to the planetary surface) than the region commonly invoked for helium rain dissolution. Thus the source for a stably stratified region out at ∼0.95 R_J remains an outstanding question.

1.2. Constraints From Jupiter's Magnetic Field

Above, we highlighted ongoing challenges between formation models and in situ gravity analysis. In this paper, we attempt to resolve these open questions by drawing from a complementary discipline: the study of planetary magnetic fields (dynamos). These fields are highly sensitive to many unique aspects of a planet's interior structure; in particular, the morphology and time-variation of planetary dynamos are very sensitive to the flow dynamics within a planet–including which regions are convective versus which are stably stratified. Thus, planetary magnetic field studies are particularly well-suited to investigating the presence and extent of stably stratified layers (SSLs) within Jupiter.

While Jupiter's magnetic field is primarily dipolar, the NASA Juno Mission has revealed additional complexity that is challenging to explain. Specifically, the field has strong north-south asymmetry (Moore et al., 2018). It is also dominated by a small number of regions with highly intense, localized field features such as the Great Blue Spot (Connerney et al., 2018; Moore et al., 2017) which may be sheared by the planet's zonal winds over time (Connerney et al., 2021; Moore et al., 2019). Previous dynamo models featuring an interior structure consisting of a solid inner core and a fully convective hydrogen shell tend to result in magnetic fields that are either too dipolar or too multipolar (Dietrich & Jones, 2018; Duarte et al., 2018; Jones, 2014). This is inconsistent with the intermediate-level complexity in Jupiter's magnetic field as observed by Juno. Overall, this suggests the need for alternative interior models, such as those with SSLs due to a dilute core (at the center of planet) and/or helium-depleted hydrogen near the H/He phase transition region (shallower).

SSLs have been shown to significantly impact the morphology of planetary magnetic fields in three-dimensional magnetohydrodynamic (dynamo) simulations. Specifically, a bottom liquid SSL has been shown to add complexity to magnetic fields, possibly explaining the multipolar natures of the fields of Uranus and Neptune (Stanley & Bloxham, 2004, 2006). Similarly, the possibility of upper stable stratification has been shown to be a plausible mechanism for axisymmetrizing the magnetic field of Saturn (Stanley, 2010; Stevenson, 1982; Yan & Stanley, 2021). However, these simulations were carried out in the Boussinesq approximation, which neglects the effects of compressibility. This approximation may be valid for Earth, where pressure-dependent effects may
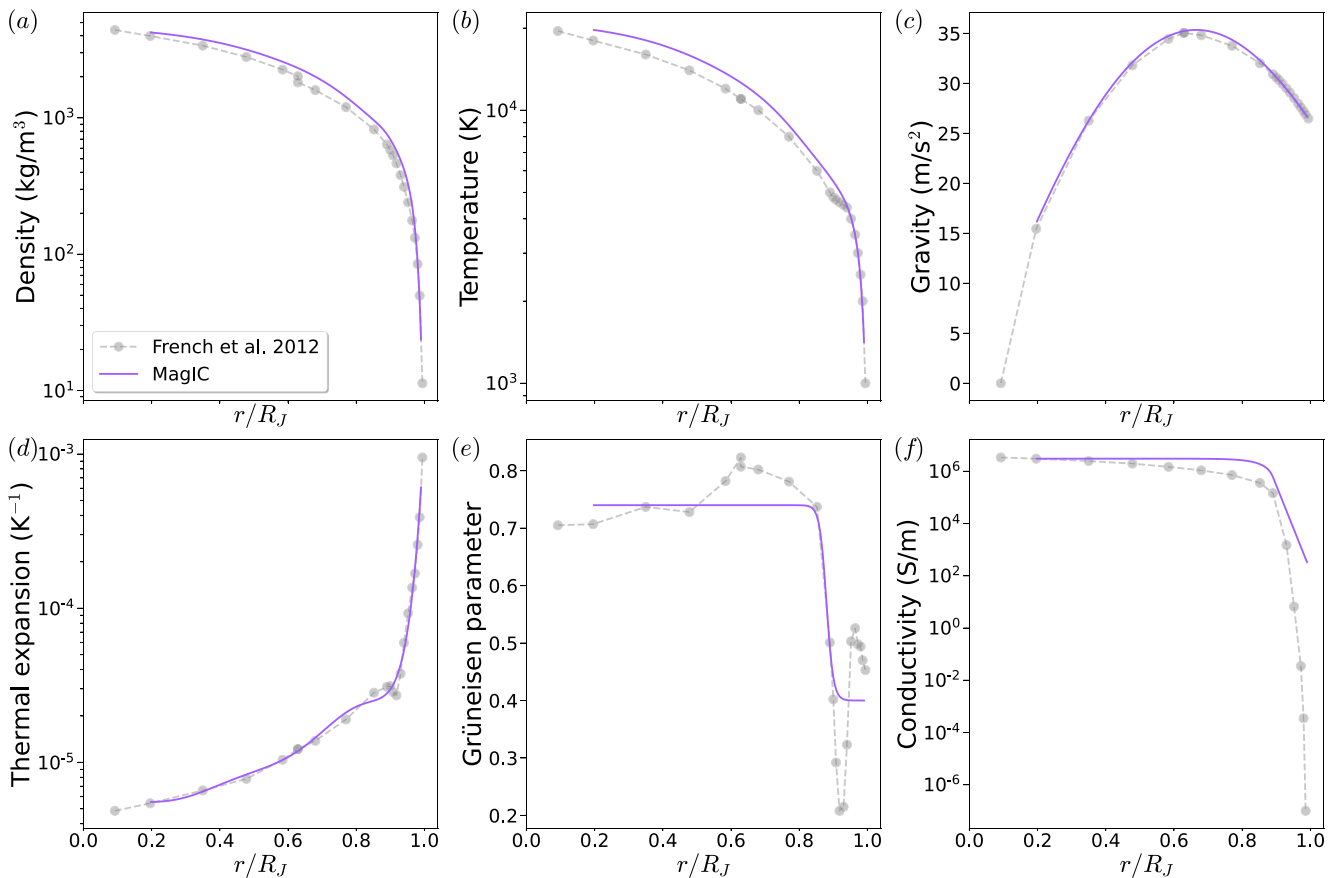
Figure 2. *Jupiter interior model properties*. Blue lines represent the properties of the Jupiter reference background profiles used in our dynamo simulations, while gray lines/dots represent the model of French et al. (2012) for comparison. Note that MagIC internally normalizes all interior quantities by the value at the outer boundary of the spherical shell, except for electrical conductivity for which it uses the value at the inner boundary. We use a cutoff radius of 0.99 R_J. (a) Density, (b) Temperature, (c) Gravity, (d) Coefficient of thermal expansion, (e) Grüneisen parameter, and (f) Electrical conductivity.

only be on order of 10%. However, these effects can be more significant for giant planets like Jupiter, where the density varies by several orders of magnitude throughout the planet (See Figure 2).

The capability to model SSLs was recently incorporated into the open-source dynamo code, MagIC (Gastine & Wicht, 2021); that work included a single proof of concept Jovian simulation in the anelastic (compressibility-dependent) approximation, which demonstrated that stable stratification has a strong influence on the dynamics of Jupiter's atmospheric jets and dynamo field. The specific stable layer simulated (∼0.85–0.9 R_J) resulted in a magnetic field that is too dipolar. Here we revisit this problem in more depth by testing a wider variety of layer placements, guided by hypotheses from Jovian interior structure and accretion models.

1.3. Overview

In this work, we perform state-of-the-art magnetohydrodynamic (MHD) simulations (dynamo models) of Jupiter's magnetic field morphology to constrain the location and extent of stable stratification within the planet. Specifically, we focus on two potential regions of stable stratification: (a) an upper stable layer (within the bounds of 0.8–0.95 R_J) and (b) a deep layer within 0–0.5 R_J. While these features may be present in a variety of dynamical forms—fully convective, layered convection, semi-convection, and/or SSL(s)—we specifically focus on the role of stable stratification in this work, due to its profound implications for Jupiter's thermal evolution. Our goal is to constrain Jupiter's present-day interior dynamics, in order to provide an important basis of comparison with the results of accretion models. Of key interest is determining if a stably stratified dilute core needs to extend beyond 0.2 R_J in order to explain Jupiter's magnetic field, which would pose a direct challenge to traditional planetary formation scenarios (Müller et al., 2020).

2. Methods

We seek to numerically simulate the MHD processes of Jupiter's interior, including the generation of its dynamo magnetic field and zonal winds. In particular, we model the extent of SSLs in the planet's interior, in order to investigate the role of key hypothesized features such as a stratified, inhomogeneous dilute ("fuzzy") core and a hydrogen-helium immiscibility zone. Thus, we choose a cutting-edge, open-source numerical dynamo code, MagIC (Gastine & Wicht, 2012; Jones et al., 2011), which recently added the capability to model the effects of stably stratified fluid layers (Dietrich & Wicht, 2018; Gastine & Wicht, 2021; Gastine et al., 2020). MagIC utilizes a pseudo-spectral approach with a poloidal-toroidal decomposition. The radial grid is determined by zeros of a Chebyshev polynomial. This results in a higher density of grid points near the upper and lower boundaries of the fluid shell, in order to help resolve boundary layers. We describe the numerical setup of the problem and our model parameter choices below.

2.1. Formulation of the MHD Problem

2.1.1. Background Reference Model

MagIC models the time-evolution of the dimensionless fluid velocity, $\mathbf{u}$, and magnetic field, $\mathbf{B}$, inside a spherical shell with rotation rate Ω. Specifically, it solves the conservation equations for momentum (Navier-Stokes), magnetic induction, and energy. The system is represented in terms of small perturbations around a static, spherically symmetric background reference state, that is,

$$\frac{|T'|}{|\tilde{T}|} \sim \frac{|\rho'|}{|\tilde{\rho}|} \sim \frac{|p'|}{|\tilde{p}|} \; \cdots \ll 1 \tag{1}$$

We use the convention of tildes to represent the properties of the background state and primes to represent fluctuations throughout. The background state quantities are in general non-dimensionalized by their values at the outer boundary of the shell.

For most quantities, we use MagIC's built-in Jupiter reference model, JUP (with adjustments to ensure dipolar fields and force stable stratification, to be described). Overall this model is a polynomial fit approximation to the adiabatic Jupiter interior model of French et al. (2012), which features a homogeneous, enriched envelope out to $0.63 \, R_J$ (see Figure 2). Note that the original background interior model technically has an abrupt, discontinuous jump in composition (Z and helium) and entropy, which would create an infinitesimally thin stratified region. However, these effects are smoothed over by the polynomial fit, and are usually not modeled directly. The radially varying electrical conductivity profile is super-exponential; see Figure 2. The outer boundary of our model is at $0.99 \, R_J$ due to steep variations in the background profiles which are difficult to resolve numerically beyond this radius. The variation in thermal conductivity in the French et al. (2012) profiles is limited to a factor of about 60 and is thus neglected, following Gastine, Wicht, et al. (2014) and Gastine and Wicht (2021). The electrical conductivity ($\tilde{\sigma}(r)$) profile from French et al. (2012) is shown in Figure 2f. It shows that the transition from a highly conductive metallic region to a semi-conducting fluid region takes place around $r/R_J \approx 0.9$. To approximate this behavior, we use a formulation introduced in Gómez-Pérez et al. (2010),

$$\tilde{\sigma}(r) = 1 + (\tilde{\sigma}_m - 1)\left(\frac{r - r_i}{r_m - r_i}\right)^{\xi} \quad \forall \quad r < r_m$$
$$\tilde{\sigma}(r) = \tilde{\sigma}_m \exp\left[\xi \frac{r - r_m}{r_m - r_i}\left(\frac{\tilde{\sigma}_m - 1}{\tilde{\sigma}_m}\right)\right] \quad \forall \quad r \geq r_m. \tag{2}$$

Thus, the interior is approximated as a combination of a nearly constant conductivity profile in the metallic region followed by an exponential fall off. $\tilde{\sigma}_m$ is the electrical conductivity of the fluid at the transition radius r_m. The conductivity is normalized to its value at the inner boundary of the simulation. We use values of $\sigma_m = 0.2$, $r_m = 0.9$, and $\xi = 13$ for all our simulations.

2.1.2. Anelastic MHD Equations

Applying the reference state described in Section 2.1.1, we use the anelastic approximation of the MHD equations (Braginsky & Roberts, 1995; Gilman & Glatzmaier, 1981; Lantz & Fan, 1999). In this formulation, the time rate of change of density perturbations relative to the background state is assumed to be small compared to changes in

the velocity—that is, sound waves are filtered out. Resolving sound waves in our models would require substantially higher time-resolution, and is not required for the goals of our study. The resulting anelastic equations are:

$$\nabla \cdot (\tilde{\rho}\mathbf{u}) = 0 \tag{3}$$

$$\nabla \cdot \mathbf{B} = 0 \tag{4}$$

$$\frac{D\mathbf{u}}{Dt} + \frac{2}{\mathrm{Ek}}\mathbf{e_z} \times \mathbf{u} = -\nabla\left(\frac{p'}{\tilde{\rho}}\right) + \frac{1}{\mathrm{EkPm}\tilde{\rho}}(\nabla \times \mathbf{B}) \times \mathbf{B} - \frac{\mathrm{Ra}}{\mathrm{Pr}}\tilde{\alpha}\tilde{T}gs' + \frac{1}{\tilde{\rho}}\nabla \cdot \mathbf{S} \tag{5}$$

$$\frac{\partial \mathbf{B}}{\partial t} = \nabla \times \left(\mathbf{u} \times \mathbf{B} - \frac{\tilde{\lambda}}{\mathrm{Pm}}\nabla \times \mathbf{B}\right) \tag{6}$$

$$\tilde{\rho}\tilde{T}\left(\frac{Ds'}{Dt} + u_r\frac{d\tilde{s}}{dr}\right) = \frac{1}{\mathrm{Pr}}\nabla \cdot \left(\tilde{\rho}\tilde{T}\nabla s'\right) + \frac{\mathrm{Pr}\,\mathrm{Di}}{\mathrm{Ra}}\left(Q_\nu + Q_\lambda\right) \tag{7}$$

where $D/Dt = \partial/\partial t + \mathbf{u} \cdot \nabla$ is the material derivative. S is the traceless rate-of-strain tensor:

$$S_{ij} = 2\tilde{\rho}\left(e_{ij} - \frac{1}{3}\frac{\partial u_i}{\partial x_i}\right) \tag{8}$$

$$e_{ij} = \frac{1}{2}\left(\frac{\partial u_i}{\partial x_j} + \frac{\partial u_j}{\partial x_i}\right) \tag{9}$$

and Q_ν and Q_λ are the viscous and Ohmic heating terms, respectively:

$$Q_\nu = 2\tilde{\rho}\left[\sum_{i,j} e_{ij}e_{ji} - \frac{1}{3}(\nabla \cdot \mathbf{u})^2\right] \tag{10}$$

$$Q_\lambda = \frac{\tilde{\lambda}}{\mathrm{EkPm}^2}\mathbf{j}^2 \tag{11}$$

In the above equations, length is non-dimensionalized using the spherical shell thickness, $d = r_o - r_i$, timescale has been non-dimensionalized by the viscous diffusion time d^2/ν, the velocity by ν/d, the magnetic field by $\sqrt{\Omega\mu_0\lambda_i\rho_o}$, and the entropy perturbations by $d|ds/dr|$ at the outer boundary of the shell. We also use the non-dimensional parameters:

Rayleigh,

$$\mathrm{Ra} = \frac{\alpha_o T_o g_o d^4}{c_p \nu \kappa}\left|\frac{ds}{dr}\right|_o \tag{12}$$

Ekman,

$$\mathrm{Ek} = \frac{\nu}{\Omega d^2} \tag{13}$$

Prandtl,

$$\mathrm{Pr} = \frac{\nu}{\kappa} \tag{14}$$

the magnetic Prandtl number,

$$\mathrm{Pm} = \frac{\nu}{\lambda_i} \tag{15}$$

and the dissipation number, Di,

$$\mathrm{Di} = \frac{a_0 g_0 d}{c_p} \tag{16}$$

The final system of equations is solved directly for the 3D fluid velocity and magnetic fields as a function of time, given the initial background profile and a small initial random perturbation.

2.2. Stable Layer Implementation

MagIC currently provides the functionality to model planetary dynamos with SSLs. Our description of the methodology used in MagIC closely follows that of the anelastic Jovian study, Gastine and Wicht (2021). Mathematically, MagIC implements SSLs by modifying the background entropy gradient, $\frac{d\tilde{s}}{dr}$ to allow for non-adiabatic reference states (perturbations are assumed to be small to preserve the validity of the anelastic approximation). An SSL is created by setting the entropy gradient to a constant value relative to the background reference state,

$$\frac{d\tilde{s}}{dr} = \Gamma_s \tag{17}$$

where Γ_s is the "degree of stratification," and is set as a free parameter. Effectively, this forces stable stratification in regions where the entropy gradient, $\frac{d\tilde{s}}{dr} > 0$. The degree of stratification is related to the Brunt-Väisälä frequency in the stable layer by

$$\frac{N}{\Omega} = \max_r \sqrt{\tilde{\alpha}(r)\tilde{T}(r)\tilde{g}(r)\frac{RaEk^2}{\mathrm{Pr}}\Gamma_s} \tag{18}$$

A constant dimensionless entropy gradient of $\frac{d\tilde{s}}{dr} = -1$ is imposed in the surrounding convective regions.

The entropy gradient of the SSL is connected smoothly to the surrounding regions with a hyperbolic tangent function. The current version of MagIC allows for SSLs to be placed either at the outer boundary of a spherical fluid shell or somewhere in the interior of the planet (i.e., sandwiched between two regions of convective fluid; see Figure 3b). For an SSL extending from non-dimensional radii r_{strat} to $[r_{\text{strat}} + h]$ (where h is the non-dimensional thickness), the two gradients are smoothly connected as follows:

$$\frac{d\tilde{s}}{dr} = \frac{1+\Gamma_s}{4} \left[1 + \tanh\left(\zeta_s \left(r - r_{strat}\right)\right)\right] \left[1 - \tanh\left(\zeta_s \left(r - r_{strat} - h\right)\right)\right] - 1 \tag{19}$$

where ζ_s is the stiffness of the transition between the stably stratified and convective layers.

In addition to utilizing the existing functionality for interior (sandwiched) stable layers (also referred to as "upper" layers in this paper, due to their simulated location within Jupiter), we added new functionality to the code to enable simulation of SSLs extending all the way to the bottom of the fluid shell (see Figure 3c). We parameterize this new option for a bottom stable layer similarly to the above. Here the planet is assumed to have a stable layer extending between the inner boundary and r_{strat}. Note that whereas in the sandwich-stratification case r_{strat} represented the bottom boundary of the layer, here it represents the upper boundary. This choice was made to minimize modifications to the shared community code.

Just as above, the bottom-stratified layer implementation is defined by a constant positive entropy gradient throughout $\left(\frac{d\tilde{s}}{dr} = \Gamma_s\right)$, and the overlying convective layer has a constant dimensionless entropy gradient of $\frac{d\tilde{s}}{dr} = -1$. The two gradients are smoothly connected as follows:

$$\frac{d\tilde{s}}{dr} = \Gamma_s - \frac{1+\Gamma_s}{2} \left[1 - \tanh\left(\zeta_s \left(r_{strat} - r\right)\right)\right] \tag{20}$$

While somewhat ad hoc, forcing stratification is standard in the solar and planetary fluid dynamic literature, and provides a controlled way to examine the effects of stratification on the resulting flows generated inside the planet. (See Takehiro and Lister (2001) and Gastine et al. (2020) for implementation in geodynamo models, and Dietrich and Wicht (2018) for an application to Saturn). We note that this approach also approximates the planet as a single-component fluid, when in reality the stratification would likely be due to chemical gradients of multiple components including H, He, and heavier elements in the planet.
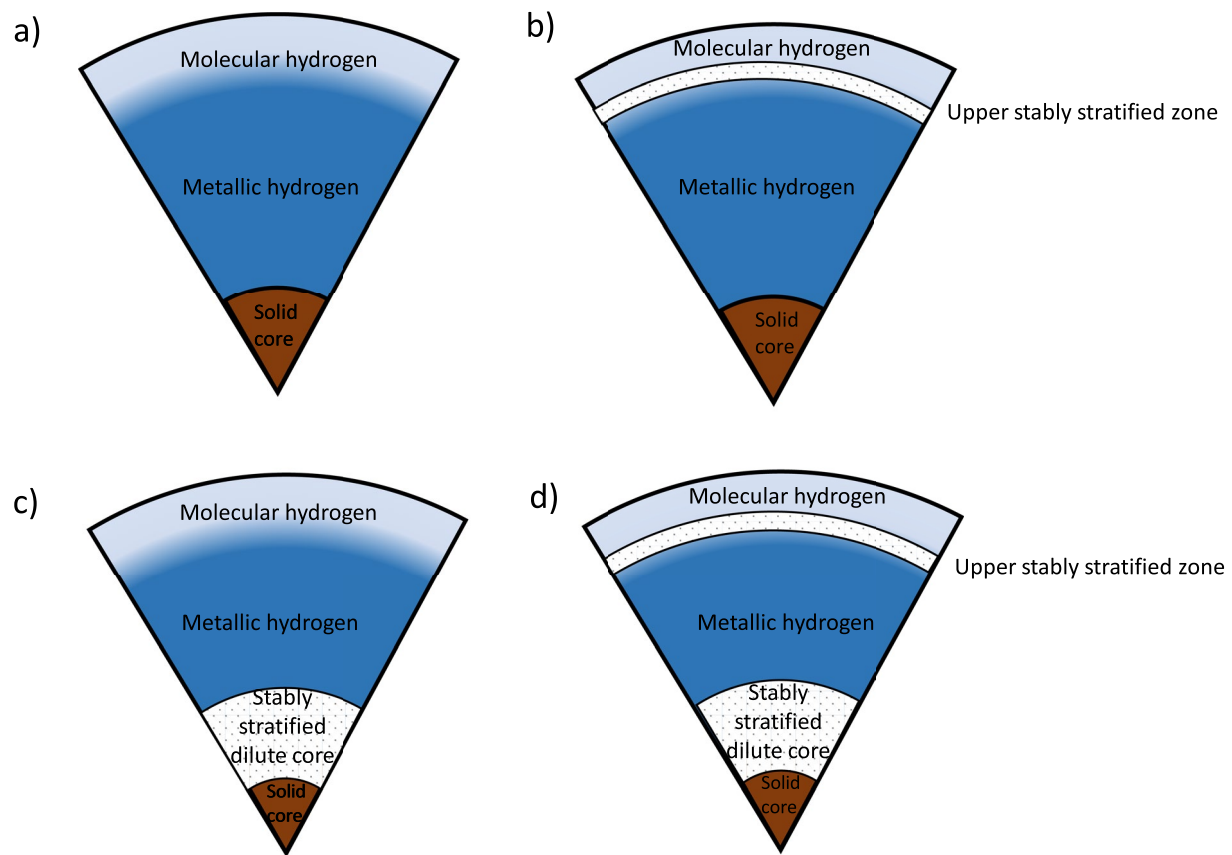
Figure 3. *Illustrations of numerical experiment cases.* (a) Baseline control model: a fully convective (traditional) interior structure featuring a compact central core. (b) A model featuring an upper stably stratified layer (SSL). (c) A "Dilute Core" model featuring an extended core region (consisting of a solid inner core from 0 to 0.2 R_J for numerical stability, with an overlying liquid SSL). (d) A "Combo DC/UP" model featuring both an upper SSL and a dilute core with extended stably stratified regions. *With the exception of the solid inner core, the exact placement and thickness of each layer in this study varies by specific model case.*

2.3. Jovian Numerical Experiments

Using MagIC, we perform several numerical experiments to explore the dynamics of Jupiter's interior. Our experimental design is largely influenced by the nature of dynamo modeling, which is extremely computationally expensive. This is especially true at the resolution levels required to model the pressure-dependent interiors of giant planets. Thus, we perform a tightly focused study.

Since we can only perform a limited number of simulations due to computational resource constraints, we focus our experiments on a small number of parameters. Several previous studies have already explored the effect of various non-dimensional fluid dynamic parameters such as the Rayleigh number (Ra), Ekman number (Ek), Prandtl number (Pr), magnetic Prandtl number (Pm), and Rossby number (Ro); as well as the broader effects of the background interior models (ranging from idealized polytrope number to more "realistic" Jupiter interiors like that of French et al. (2012)); and the role of different electrical conductivity profiles (i.e., different metalization depths/drop-off rates) and heating models (internally heated vs. top-down cooling). Thus, we rely on the important conclusions those authors have derived (see Duarte et al. (2018) for a review), and do not repeat those parameter surveys here. Instead, we focus on the effect of large-scale changes to Jupiter's interior structure: the role of stable stratification due to a possible dilute core and/or helium rainout. See Table 1 for a list of our numerical dynamo simulation cases.

2.3.1. Baseline Control Models

To understand the effect of these new possible interior structures, we first perform a single "dipolar baseline" control model run using a traditional Jupiter interior structure (a solid compact core from 0 to 0.2 R_J, and no stratified regions), similar to the models of Duarte et al. (2018); see Figure 3a. The cutoff radius of 0.2 R_J

Table 1
Overview of Dynamo Simulations

Model name	Solid core radius (R_J)	SSL (R_J)	N/Ω	Γ_s	Magnetic field morphology	Lowes spectrum RMSLE
Dipolar baseline	0.2	N/A	N/A	N/A	Dipolar	0.70
Multipolar baseline	0.2	N/A	N/A	N/A	Multipolar	3.22
Dilute core 0.25	0.2	0.2–0.25	10.01	1500	Multipolar	2.97
Dilute core 0.3	0.2	0.2–0.3	10.04	1300	Multipolar	2.90
Dilute core 0.4	0.2	0.2–0.4	10.00	980	Multipolar	2.67
Dilute core 0.5	0.2	0.2–0.5	10.09	800	Multipolar	3.83
Solid dilute core 0.4	0.4	N/A	N/A	N/A	Multipolar	2.65
Upper SSL 0.80–0.85	0.2	0.80–0.85	9.10	450	Dipolar	1.44
Upper SSL 0.85–0.90	0.2	0.85–0.90	9.13	530	Dipolar	0.63
Upper SSL 0.90–0.95	0.2	0.90–0.95	9.08	310	Bistable	0.41 (D)
						1.89 (M)
Upper SSL 0.80–0.90	0.2	0.80–0.90	9.10	450	Dipolar	1.30
Upper SSL 0.85–0.95	0.2	0.85–0.90	9.79	360	Dipolar	0.62
Upper SSL 0.80–0.95	0.2	0.80–0.95	9.79	360	Dipolar	1.27
Combo DC/UP 0.80–0.85	0.4	0.80–0.85	9.10	450	Multipolar	2.09
Combo DC/UP 0.85–0.90	0.4	0.85–0.90	9.13	530	Dipolar	0.77
Combo DC/UP 0.90–0.95	0.4	0.90–0.95	9.08	310	Multipolar	2.76
Combo DC/UP 0.80–0.90	0.4	0.80–0.90	9.10	450	Multipolar	2.15
Combo DC/UP 0.85–0.95	0.4	0.85–0.95	9.79	360	Multipolar	2.24
Combo DC/UP 0.80–0.95	0.4	0.80–0.95	9.79	360	Dipolar	1.78

Note. Here we provide a list of dynamo simulations in our case study. The models are of four classes (aligned with Figure 3): fully convective models ("baseline"), models featuring an upper SSL ("Upper SSL"), models with a stably stratified dilute core ("Dilute core"), and combination models with both an upper and lower stably stratified regions ("Combo DC/UP"). While the table highlights parameters that differ between models, many parameters are the same across simulations. For example, all of our models use non-dimensional fluid parameter values of Ra = 8×10^7 (except the multipolar baseline model which uses Ra = 1.8×10^8), Ek = 10^{-4}, Pr = 1, Pm = 3, and a simulation upper cutoff radius of 0.99 R_J. All simulations use a grid resolution of $N_r = 161$, $N_\theta = 384$, and $N_\phi = 768$ grid points in the radial, meridional, and azimuthal axes respectively. Models including a stably stratified layer use a stratification slope of $\zeta_s = 130$. The degree of stratification, Γ_s, was fixed to give a maximum N/Ω ratio of approximately 10 in the stratified layer. Here RMSLE stands for root mean square log error.

was specifically chosen as the maximum radius considered plausible by traditional accretion models (Müller et al., 2020). Our dipolar baseline model uses a Rayleigh number Ra = 8×10^7, Ek = 10^{-4}, Pr = 1, and Pm = 3. This model was based on Case 34 of (Duarte et al., 2018), but with a slightly higher Rayleigh number. We also use a grid resolution of $N_r = 161$, $N_\theta = 384$, and $N_\phi = 768$ grid points in the radial, meridional, and azimuthal directions respectively, leading to a maximum spherical harmonic degree $l_{max} = 256$. All of our simulations also used these same simulation control properties, with the exception of the Rayleigh number for our multipolar baseline model. We chose to keep most values the same in each simulation, and focused on varying the core radius, and the locations and thicknesses of SSLs.

We acknowledge the common concern that computational restrictions require an unphysically large Ekman number for planetary studies (i.e., too viscous). Some works have hinted at the possibility of different dominant force balances only seen at lower Ekman numbers (Yadav et al., 2016); whether this is consistently the case remains to be seen. However, stably stratified models require significantly higher grid resolutions than traditional compact core models, and so reaching these low Ekman numbers is an even greater challenge here. We choose instead to perform a broader suite of models with a higher Ekman number (Ek = 10^{-4}) that is commonly used in the literature. This represents a balanced approach, and allows us to easily compare the effects of our stably stratified models with both our baseline models and previous models produced by the scientific community.

Our baseline simulation was consistently dipolar for the entire run time period. This baseline model was then used as the initial checkpoint for our simulations with SSLs. We also perform a "multipolar baseline" control model

using identical parameters as the dipolar baseline, with the exception of a higher Rayleigh number (1.8×10^8) to yield a multipolar model.

2.3.2. Dynamo Models With Stratified Interiors

After creating our baseline comparison models, we perform a series of dynamo simulations featuring a stably stratified dilute core (referred to here as "Dilute Core models" throughout the text, although in reality dilute cores need not be stratified). Our models are simulated as a solid inner core from 0 to 0.2 R_J, with a fluid stably stratified region overlying the solid inner core (see Figure 3c); the presence of the inner core provides our models with numerical stability. Specifically, we simulate models with total non-convective core radii (solid inner core plus liquid SSL) out to 0.25, 0.3, 0.4, and 0.5 R_J. We performed exploratory simulations with bottom SSLs extending to even higher radii, but the initial results of these simulations were too similar to our other stratified dilute core models to justify the additional expenditure of computational time within our limited parameter study. Overall, our dilute core cases provide a strong contrast with our baseline cases, which only have a total core radius of 0.2 R_J—the maximum radius permitted by traditional accretion models (Müller et al., 2020). As a control, we also perform a simulation with a large, entirely solid core (i.e., no SSL) ranging from 0 to 0.4 R_J. We note that while we only test the case of a dilute core that is entirely non-convective here (i.e., solid or stably stratified across the entire volumetric region), additional geometries such as multilayered or fully convective dilute cores may be possible (Militzer et al., 2022).

For all of our dilute core models, the extent of the SSL was chosen first, and then the degree of stratification was set inside that region to yield a maximum Brunt-Väisälä frequency $N/\Omega \approx 10$ in the stratified region. This value was used so as to be directly comparable to the case by Gastine and Wicht (2021). While the true value inside Jupiter may be closer to 1–3 for upper SSLs depending upon the interior model chosen (see Miguel et al. (2016), Debras and Chabrier (2019), and Gastine and Wicht (2021) for details), the increased stiffness of the SSL helps balance out the effect of the artificially enhanced viscosity in dynamo models due to numerical limitations. We did perform initial probing studies using a more weakly or strongly stratified dilute core ($N/\Omega \approx 0.5$ or 100, respectively). Models with higher values of N/Ω appear to have stronger propagation of internal gravity waves in the core, which could have implications for observations of the planet's interior modes by the Juno spacecraft or telescopic observatories. However, the degree of stratification in the dilute core did not significantly impact the primary concern of our study—the morphology of the magnetic field at the planetary surface—so we do not consider it further here.

We also performed simulations featuring an upper SSL ("Upper SSL" models). Our experiments explored layers with thicknesses of 0.05, 0.1, and 0.15 R_J (between 3,500 and 11,000 km in thickness), and a variety of depths (such that the layer was fully encompassed within the radial region between 0.8 and 0.95 R_J; see Figure 3b). An upper SSL may be caused by helium rainout near the outer boundary of the dynamo region. In such case, the layer thickness and depth would be directly determined by the planet's temperature, pressure, and electrical conductivity profiles. However, the H/He mixing phase diagram has sufficient uncertainty that we treat these values as free parameters, both for exploring Jupiter's magnetic field as well as gaining general insight about the effects of SSLs in giant planets. We note that an outer extent of 0.95 R_J for He rainout is shallower than predicted by all current H/He phase diagrams, but we include it here as an outer bound due to suggestions from previous magnetic field analyses that it is a radius of interest (Christensen et al., 2020; Moore et al., 2019). We discuss the interesting contrast between the locations of possible stratified layers suggested by high pressure physics models of hydrogen-helium gradients versus evidence from other disciplines like seismology and magnetic field analysis more in Section 4; it is possible that multiple processes causing stable stratification may be at play.

Finally, we performed combination simulations of models including both an extended dilute core and an upper SSL (possibly due to helium rain); see Figure 3d. Such models are denoted as "Combo DC/UP" models throughout the text. The upper layers in these cases were simulated identically to those described above, while the dilute core region was modeled as a large solid inner core for simplicity. This choice is justified by our results (See Section 3), which find no significant differences in field morphology between dilute core models with a purely solid inner core versus those with a bottom SSL.

We note that we have chosen to idealize the possible dilute core within Jupiter as a stratified layer overlying a small compact core (or, for comparison, as a large and entirely solid core region), and the hypothesized helium immiscibility zone as an upper stratified layer. In reality, the dynamics of these features may be

further complicated by alternative processes such as layered convection (Moore et al., 2018), marginal stability, or semiconvection/double-diffusive convection (Leconte & Chabrier, 2013; Nettelmann et al., 2015), that is, a region that is compositionally stable but thermally unstable. Consideration of these processes is beyond the scope of our current study, but would be a fruitful and important direction for future research in the field.

3. Results

In this study, we explore whether adding complexity to Jupiter's interior structure (i.e., a stably stratified dilute core and/or a possible helium rainout zone) could help explain the planet's observed magnetic field morphology. That is to say, we seek a "Goldilocks" or intermediate dynamo model—whereby starting with a dipolar baseline case and adding new interior features, we manage to add a small amount of necessary complexity to bridge the two end-member regimes.

We primarily focus on the broad implications of time-averaged properties (details are described below). Planetary dynamo models are turbulent and may vary strongly in time; similarly, observational data has also found evidence of time-variation in Jupiter's actual magnetic field (Moore et al., 2019). Working with averaged quantities helps to prevent biased conclusions from possibly unrepresentative "snapshots" of the field at isolated moments in time. Resolving the time-dependence of features such as isolated flux spots like the Great Blue Spot in a statistically meaningful manner requires longer simulation run times and is computationally expensive; we hope to follow up on our promising candidate models in a future study.

3.1. Magnetic Field Morphology

First, we examine the magnetic field morphology of our numerical simulations. A planet's dynamo magnetic field at the surface can be represented as a potential field, V, with degree l and order m spherical harmonic coefficients, g_l^m and h_l^m:

$$V = a \sum_{l=1}^{\infty} \left(\frac{a}{r}\right)^{l+1} \sum_{m=0}^{l} P_l^m(\cos\theta) \left[g_l^m \cos(m\phi) + h_l^m \sin(m\phi)\right] \tag{21}$$

where V is a function of position relative to a planetary reference radius, a (in our case, $a = 1\ R_J = 71{,}492$ km).

3.1.1. 1D Power Spectra

Using the field coefficients at the outer boundary of our fluid dynamics simulations (0.99 R_J), we find the time-averaged Lowes power spectrum (Lowes, 1966) to compare the total power, R_l, at each spectral degree:

$$R_l = (l+1)\left(\frac{a}{r}\right)^{2l+4} \sum_{m=0}^{l} \left[\left(g_l^m\right)^2 + \left(h_l^m\right)^2\right] \tag{22}$$

The Lowes power spectrum is commonly used to estimate the location of the surface of a planetary dynamo by assuming that the dynamo source emits power as a flat spectrum, and finding the distance to this source region that best-fits the power spectrum of the observed field. This is based on geometric reasoning: the further one is from the source generating region, the more strongly higher order terms in the potential field expansion will decay relative to lower order terms (i.e., "all things resemble a dipole when observed from a far enough distance", see Equation 21). Using this method on Juno-derived magnetic field models, one would estimate that Jupiter's convective dynamo extends to between 0.81 and 0.85 R_J (Connerney et al., 2018, 2021; Sharan et al., 2022).

This method provides an excellent first approximation, but is largely empirical in nature and primarily informed by studies of Earth's magnetic field. There are no first principles requirements for dynamos to emit at a flat spectrum, and the "dynamo surface" may be poorly defined for fluid planets such as Jupiter which have radially varying conductivity profiles and possibly intricate, multilayered interiors. By performing a suite of 3D MHD simulations, we can compare the data-derived power spectrum to the specific spectra resulting from a range of realistic scenarios for Jupiter's interior.

After initializing each dynamo model from our dipolar baseline checkpoint file, we allowed the simulations to stabilize for 0.9 viscous diffusion times (0.3 magnetic diffusion times for Pm = 3, similar to other works). Then
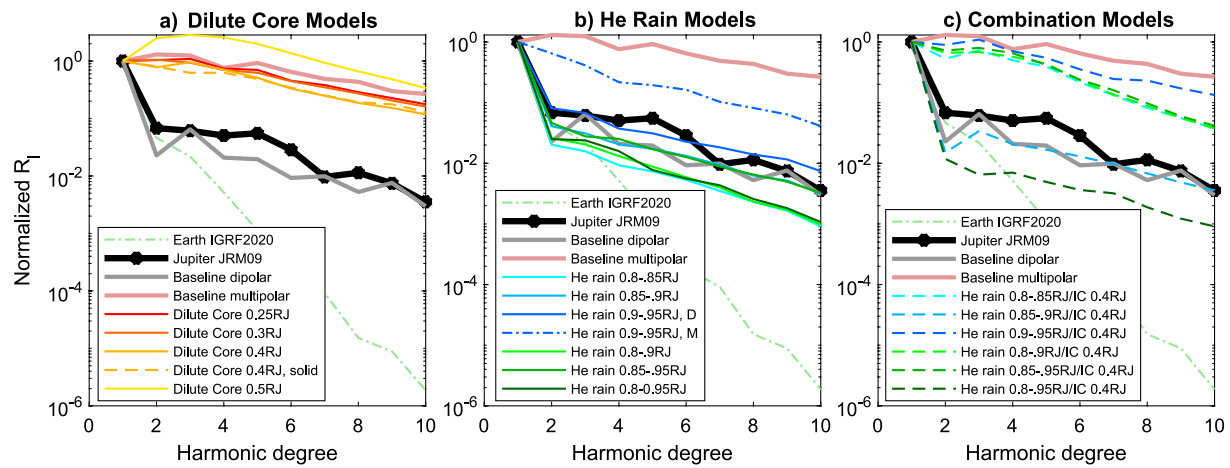
Figure 4. *Time-averaged Lowes power spectrum.* We compare the time-averaged Lowes power spectra of our dynamo models to the Juno JRM09 model (Connerney et al., 2018). All spectra have been normalized to the power in the dipolar term. We also show the power spectrum of Earth's dynamo field using the IGRF-13 model for comparison (Alken et al., 2021). (a) *Dilute core models.* (b) *Upper stably stratified layer (SSL) models.* (c) *Combination models with both an extended, stably stratified dilute core and an upper SSL.*

we calculated the time-averaged Lowes spectrum for the remainder of the simulation period, normalized to the power in the main dipole. We note that all dipolar models in our study were relatively steady, while all multipolar models underwent frequent reversals.

Figure 4 compares the resulting power spectra of our dynamo simulations (colored lines) to the JRM09 magnetic field model (Connerney et al., 2018) derived from Juno spacecraft observations (black line), and is summarized in Table 1. We also show Earth's power spectrum using the IGRF-13 model for comparison (Alken et al., 2021). Earth's power spectrum has a much faster falloff with degree than Jupiter's due to the deeper depth of its dynamo region relative to planetary radius ($\sim$0.55 R_E vs. $\sim$0.85–0.95 R_J). Our dipolar and multipolar baseline models reproduce the two end-member regimes observed in the literature for compact core models, as expected. In particular, our choice of dipolar baseline model is a surprisingly reasonable fit to the power spectrum of JRM09, although it has a significant mismatch in the power of the quadrupolar term.

3.1.1.1. Dilute Core Models

Like traditional compact core models, models including SSLs still appear to fall into the end-member extremes of highly dipolar or highly multipolar morphologies. Past dynamo modeling studies of Uranus and Neptune's interiors in the Boussinesq limit (Stanley & Bloxham, 2006) had found that larger inner core sizes lead to increased field complexity; models with intermediate shell thickness somewhat resembled Jupiter's field. Thus, we had initially expected that the inclusion of a non-convective dilute core region of the correct radius could lead to a case with intermediate morphology, but our results do not support that hypothesis. Instead, our non-convective dilute core models unanimously yield multipolar magnetic field morphologies (red/orange/yellow lines in Figure 4). This was true for all radial extents of the non-convective dilute core examined here, with larger dilute cores generally having worse root mean square log errors to the JRM09 power spectrum than smaller ones (See Table 1). Note that we did not consider interior structures with convective dynamics such as multi-layered dilute cores or double diffusive convection.

While previous studies found that dynamo models in the Boussinesq approximation are sensitive to the difference between a liquid stably stratified core and a solid inner core of the same radius (Stanley & Bloxham, 2004, 2006), no significant difference in field morphology was observed in our anelastic simulations. This is likely because the large number of density scale heights traversed in our anelastic Jupiter simulations reduces the models' overall sensitivity to the specific nature of the deep bottom boundary, aside from the general aspect ratio of the convective region. Overall we find that a fully stably stratified dilute core alone does not appear to explain Jupiter's unusual magnetic field (Moore et al., 2018).

3.1.1.2. Upper SSL Models

In contrast to the multipolar dilute core models, our models implementing an upper stably stratified region occurring somewhere between 0.8 and 0.95 R_J (Figure 3b) are primarily dipolar (Figure 4b). We find that the Lowes power spectrum appears to be strongly correlated with the location of the stable layer: shallower layers have stronger contributions from higher order terms. This trend can be explained by the stable layer's ability to change the effective "depth of the dynamo surface." In MHD simulations of Jupiter with a fully convective interior, dipolar dynamos are confined to deeper regions of the planet due to competition with the zonal winds (while multipolar dynamos are generated in more shallow regions) (Duarte et al., 2018). Here we find the stable layer provides a buffering separation zone between Jupiter's convective dynamo and its strong zonal winds, allowing for a dipolar dynamo to extend to shallower depths than might otherwise occur in the presence of strong zonal winds.

Unlike the layer placement, changing the thickness of an upper stable layer due to helium rain did not appear to affect the Lowes power spectrum significantly (see Figure 4b). Layers from 0.8 to 0.85, 0.8 to 0.9, and 0.8 to 0.95 R_J all have nearly identical power spectra, as do the layers from 0.85 to 0.9 and 0.85 to 0.95 R_J. Overall we find that the location of the bottom of the stratified layer—and not the layer thickness—appears to be the primary determining factor of the dynamo's power content. This is consistent with interpreting the power spectrum in terms of geometric distance from the primary source of field generation: the convective dynamo region. We also note that from the perspective of the magnetic Reynolds number, the bottom of an upper stable layer is likely where advective shearing of the electromagnetic field would be strongest due to the increased electrical conductivity, although this effect would also depend upon the rate of decay of fluid velocity with depth.

3.1.1.3. Combination Models

While all of our original dilute core models are multipolar, combination models that have both an extended dilute core region and an upper stable layer (Figure 3d) produce both dipolar and multipolar morphologies, depending upon layer placement (Figure 4c). As a reminder, our previous results found no significant difference between a large, extended core that is entirely solid (0–0.4 R_J) versus a core consisting of a smaller solid inner core with an overlying liquid stably stratified core (0–0.2 and 0.2–0.4 R_J, respectively). Thus for numerical convenience, our combination models simulate the dilute core region as a larger solid core extending from 0 to 0.4 R_J. We find that combination models with dipolar magnetic fields closely reproduced the original power spectrum of these models when only an upper stable layer was included (see Figures 4b–4c, models with stable layers at 0.85–0.9 and 0.8–0.95 R_J). However, other combination models were entirely multipolar. This likely represents that there is a close tipping point between dipolar and multipolar dynamo modes (as found in other studies, e.g., Duarte et al. (2018)), and that the exact placement and thickness of the stable layer(s) can push this balance one way or the other, depending upon the resulting convective aspect ratios. While bistability was not explicitly observed in any of our combination model simulations, we cannot fully rule it out either.

3.1.1.4. Best-Fitting Model

Our best-fitting model has an upper SSL extending between 0.9 and 0.95 R_J, and a traditional compact core from 0 to 0.2 R_J (Figure 3b, not to scale; see also the medium blue solid line in Figure 4b). It provides an excellent fit to the normalized JRM09 power spectrum, with near exact fits to the quadrupole and octupole terms. The fit of our upper SSL model is significantly better than our baseline dipolar compact core model (root mean square log error, or RMSLE, of 0.41 vs. 0.70). More generally, all upper SSL models with a bottom boundary starting at 0.85 R_J or shallower provide a better fit to JRM09 than the dipolar baseline model. The best-fitting model's power spectrum is smoother than JRM09, which can be explained by the time-averaged nature of our model (since JRM09 only represents the Jovian field at a specific snapshot in time).

Interestingly, our best-fitting model is also bistable. That is, it stochastically switches between a non-reversing dipolar and a reversing multipolar regime (see Figures 4 and 5). While atypical for Earth-like models, bistability is a commonly observed phenomenon in anelastic dynamo models of giant planets (Duarte et al., 2018). This is usually thought to be due to competition between the planet's dynamo magnetic field and the zonal winds. We find here, however, that this bistable competition is still observed on rare occasions even when a SSL is added as a buffer between the dynamo and the zonal winds.
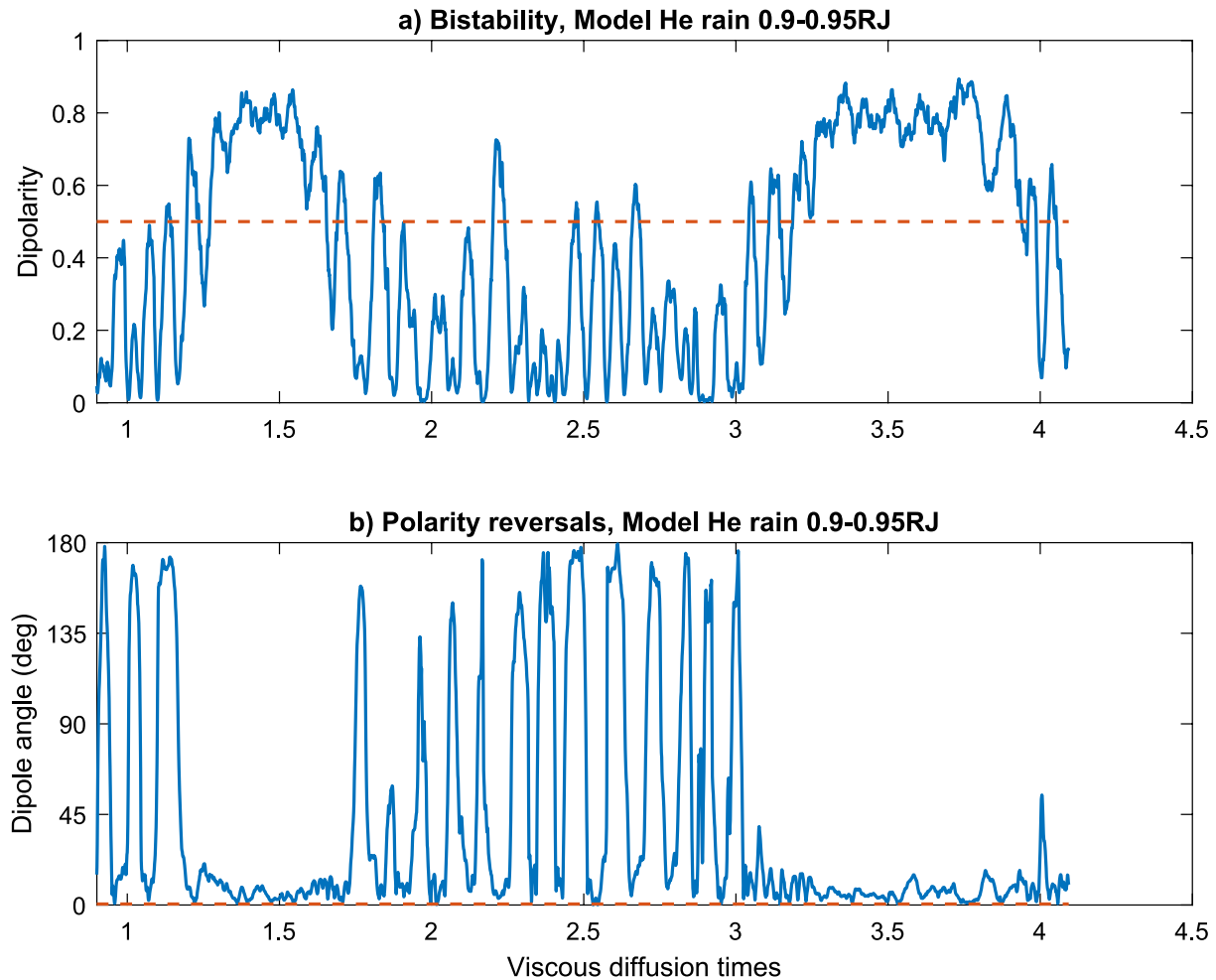
Figure 5. *Bistability of model Upper stably stratified layers 0.9–0.95 R_J.* (a) The blue line shows the dipolarity of the axial dipole at the outer boundary of the fluid shell. The model stochastically switches back and forth between dipolar and multipolar states. To separate these two modes more quantitatively, we apply a cutoff dipolarity value of 0.5 (orange line), where high dipolarity signifies a dipolar state. As with our other models, the first 0.9 viscous diffusion times of the simulation are not used in our analysis in order to allow the model to adjust from its dipolar baseline initialization state. (b) The transitions between dipolar and multipolar states are clearly demonstrated by the dynamo's pattern of polarity reversals. Our dipolar Jovian models consistently have steady magnetic polarity, while the multipolar models undergo frequent reversals.

3.2. Zonal Wind Profiles

Explaining Jupiter's atmospheric zonal wind profile alone has proved to be a decades long challenge in geophysical fluid dynamics and atmospheric science. Producing a Jovian model that has both reasonable winds and a dipolar dynamo simultaneously is an even larger challenge, due to competition between the winds and the dynamo. While the primary goal of our study is to understand the role of stable layers on the morphology of Jupiter's magnetic field, our fluid dynamic simulations also provide important insights on this secondary indicator, since our models encompass almost the full radial extent of the planet.

Previous dynamo studies implementing a compact core have typically found it challenging to simultaneously produce a dipole dominated surface field and a Jupiter-like profile of alternating zonal winds (Dietrich & Jones, 2018; Duarte et al., 2013, 2018; Gastine, Wicht, et al., 2014; Heimpel & Gómez Pérez, 2011; Jones, 2014). Our present study is in agreement with recent studies which have suggested that having a SSL between the highly conducting and non-conducting regions of a simulation helps in overcoming this obstacle (Christensen et al., 2020; Gastine & Wicht, 2021).

We find that models featuring thin, upper stable layers (possibly due to mechanisms such as helium rain) provide largely improved fits to Jupiter's time-averaged zonal winds (See Figures 6h–6k). The width of the prograde jet
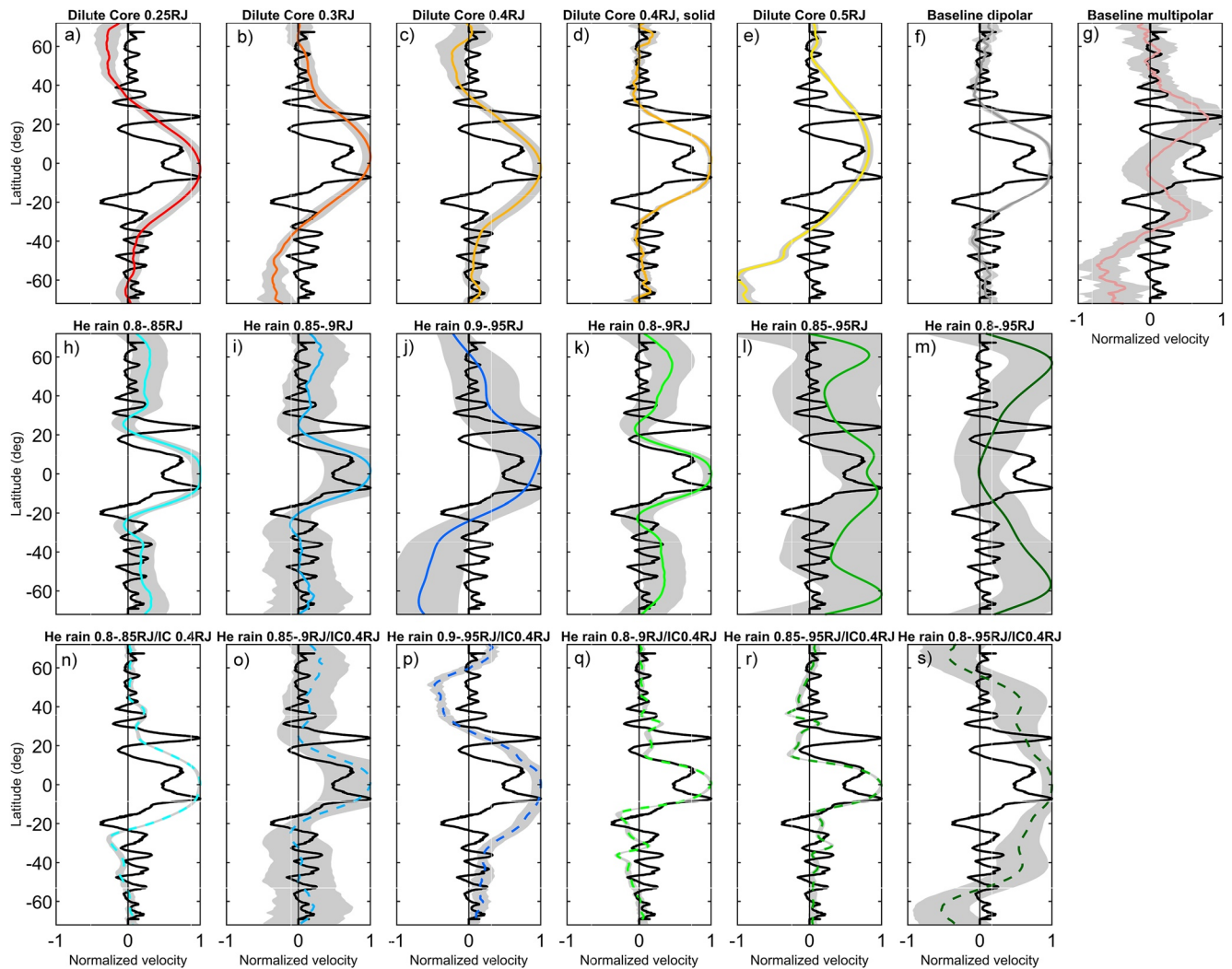
Figure 6. *Time-averaged surface zonal winds.* We compare the normalized, time-averaged zonal winds of our dynamo models at the outer boundary of the fluid shell, 0.99 R_J (colored lines). We also show the standard deviation of the normalized winds (gray shaded region), and cloud-tracking observations of Jupiter's surface zonal winds from December 2016 (approximately coincident with Juno perijove 3; thick black line) (Tollefson et al., 2017).

shrinks slightly in latitude to more closely match Jupiter's observed winds, and some models even start to replicate the weak retrograde jets near 20–30° latitude. While the wind morphology of combination models (featuring both a dilute core and upper stable layer) is slightly more varied across models, they provide similarly good fits to the observed winds (see Figures 6n–6s). This again suggests that an upper stable layer helps offset the issues caused by a stratified dilute core.

When the upper SSL is made too thick, however (e.g., 0.1–0.15 R_j; Figures 6k–6m), an unrealistically strong high latitude jet appears to dominate. At the extremes, the models become highly time-varying (large standard deviation), and the equatorial prograde jet is lost entirely. It is possible that these effects are an artifact of treating the stable layer thickness as a free parameter, when in reality it is a function of the conductivity profile. While computational limitations enforced a small parameter suite on our study, this is a rich topic for a follow-up exploration future work.

4. Discussion

In this work, we performed advanced numerical MHD simulations of Jupiter's interior, investigating the existence and extent of stably stratified regions within the planet. Specifically, we investigated stratified regions representing the effects of a possible dilute core and/or an upper stably stratified region—features postulated

by gravity observations and high pressure physics studies, and key to testing hypotheses of Jupiter's formation. Previous fully convective dynamo studies with only a compact core display a strong dichotomy of too-dipolar or too-multipolar magnetic field morphologies. Our hope was that by adding the correct combination of layer placement and thicknesses to Jupiter's interior, we would identify a dynamo model that better explains field models produced from Juno spacecraft observations.

Indeed, we find that an upper SSL does help to explain Jupiter's observed features. Such layers produced dipolar field morphologies; layers with bottoms at $0.85\,R_J$ or shallower produced better fits to Jupiter's observed power spectrum than our compact core baseline model, with the shallowest layers having the best fit of all. These models also provide slightly enhanced fits to the planet's zonal winds. Our results are consistent with trends found from dynamo explorations of Jupiter's possible conductivity profile with a compact core (Duarte et al., 2018), which also favor shallower metalization depths. Since the dynamics of hydrogen-helium immiscibility and resulting density gradients/stratified layers are intimately linked to the metalization of hydrogen, this paints a cohesive picture of the planet's interior structure and dynamics.

In contrast, we find that an extended, stably stratified dilute core alone does not appear to explain Jupiter's field. Our stably stratified dilute core models only produced multipolar magnetic fields, and yielded zonal wind profiles with too thick of a prograde jet. Thus, we find that stratified dilute core models (without any additional layering) are outmatched by fully convective/compact core models in all respects, which are usually able to somewhat match Jupiter's observed winds or observed field but not both. We also find that whether the "stratified" dilute core is fully solid or a stably stratified liquid does not appear to make a difference in the anelastic dynamo limit; while we present stratified dilute core simulations out to $0.5\,R_J$ here as part of our tightly focused case study, we also performed shorter exploratory studies out to higher radii and still found the results to be consistently multipolar.

When a stratified dilute core is present in combination with an upper SSL, however, these problems are partially resolved. While most combination models were multipolar, dipolar cases could still be found. Additionally, the planet's zonal wind profiles improved as well, yielding thinner equatorial jets more consistent with Jupiter's ground-truth.

We caution that while our evidence is strongly against the specific interior model of a stably stratified dilute core that is entirely non-convective and with no upper stable layer, more research will be required to fully rule this option out. Our study only explored a limited parameter space in conductivity and non-dimensional fluid dynamics parameters due to computational limits. Some studies have suggested that the thickness of the prograde jet may decrease at smaller Ekman numbers (Gastine, Heimpel, & Wicht, 2014; Gastine, Wicht, et al., 2014). This is unlikely to resolve the mismatch in magnetic field morphology, but it could improve the fit to Jupiter's zonal winds.

Additionally, while we assumed that Jupiter's observed surface zonal winds from cloud tracking extended deeper into the planet (i.e., to at least $0.99\,R_J$ where our fluid shell began), this may not be the case. Historically, fluid dynamical theories of Jupiter's zonal winds have fallen into two main camps—(a) that the winds extend geostrophically deep into the planet along so-called Taylor Columns (Busse, 1976), or (b) that the surface winds could be considered a shallower "weather layer" due to effects such as variable solar insolation or latent heat from ortho/para hydrogen phase transitions (see Vasavada and Showman (2005) for a review). Models of Jupiter's interior and zonal winds from Juno gravity observations suggest that the winds do extend deep (Guillot et al., 2018; Kaspi et al., 2018), rendering this latter hypothesis unlikely.

Finally, while our results cast doubt on the considered the case of a dilute core that is stably stratified across the entire region, many other flavors of a dilute core may still be possible. One possibility is a marginally stable dilute core. While we ran initial exploratory simulations and found the field morphology to be much more sensitive to the overall aspect ratio of the convective region than the stability of the bottom boundary, we cannot rule out the possibility of a marginally stable dilute core entirely and recommend it worthy of additional consideration. Other possibilities include a fully convective (i.e., homogeneous) dilute core; layered convection (e.g., featuring an outer stable region where the gradient is sharpest overlying a second interior convective region Militzer et al. (2022)), or semiconvection (Leconte & Chabrier, 2012; Moll et al., 2017). Indeed, while semi-convection traditionally operates as a staircase of hundreds to thousands of thin layers for Earth-like regimes, the dynamics of semi-convection in astrophysical regimes are poorly understood and may deviate substantially from this

model (Garaud, 2018). It is clear that an investigation of the possibility of magnetic field generation under semi-convection is required. Despite these caveats, however, our initial evidence from Jupiter's magnetic field and zonal winds is still starkly against an interior profile that has only a dilute core and no upper stratified layer.

4.1. Comparisons With Current Jupiter Interior Models

A central question of this work was to determine if a stably stratified dilute core could extend beyond 0.2 R_J in Jupiter. This is a critical metric in planetary formation modeling. Müller et al. (2020) found that traditional accretion models cannot produce models with dilute cores that have radial extents greater than 0.2 R_J, even when the models were intentionally pushed to possibly nonphysical limits in order to support the formation of an extended dilute core. That radius has proved to be a key cutoff for Jupiter's dynamo magnetic field as well; stratified dilute core radii larger than 0.2 R_J did not produce any dipolar (i.e., Jupiter-like) magnetic fields, except for when an upper SSL was also present. Thus, our results are consistent with current planetary accretion models, including new work suggestive of an interior with both a fuzzy core with an upper stable layer (Shibata & Helled, 2022).

Closer to the planet's surface, interior models constrained by Juno gravity data often require extremely low concentrations of atmospheric heavy elements (Z). One way to solve this problem is to artificially enhance the planet's surface temperature (Miguel et al., 2022; Nettelmann et al., 2021), or to assume a steeper-than-adiabatic T-gradient in an inhomogeneous stably stratified region at ∼0.95 R_J (Debras & Chabrier, 2019). Our study reports evidence from simulations of Jupiter's magnetic field morphology that strongly support an upper stratified layer in the planet's interior at this depth. The synergistic results from gravity and magnetic field analyses reported here is extremely promising. However, the exact mechanism of such a shallow SSL (0.9–0.95 R_J) is currently unknown.

One possibility worthy of consideration is helium rainout. Outstanding questions remain about the existence and extent of helium rainout within the giant planets. For example, while Saturn is currently believed to be experiencing helium rain, there is significant uncertainty regarding the extent of this process. Evolutionary models predict that Saturn should be colder (cooled more quickly since formation) than its present day temperature, and so a process such as helium rain can help to explain Saturn's slower cooling and excess luminosity (Fortney & Hubbard, 2003). Analysis of Saturnian upper atmospheric helium abundance observations vary depending on the adopted methods, from a slightly depleted state (Conrath & Gautier, 2000; Koskinen & Guerlet, 2018) (minimal helium rainout) to severely depleted (Achterberg & Flasar, 2020; Conrath et al., 1984; Sromovsky et al., 2016) (extensive helium rainout). The case for helium rain is less certain for Jupiter based on the planet's pressure temperature profile (Brygoo et al., 2021; Morales et al., 2013; Schöttler & Redmer, 2018), although atmospheric measurements of outer atmospheric helium and neon depletion from the Galileo probe strongly suggest the presence of helium rain (Niemann et al., 1998).

But our preferred depth for the upper SSL, 0.9–0.95 R_J, is much shallower than current phase diagrams of H/He mixtures suggest helium rain should occur. While there are large uncertainties in the exact location of H/He demixing, models consistently find it should be in the vicinity of 0.6–0.86 R_J, or 0.9–10 Mbar (Hubbard & Militzer, 2016; Mankovich & Fortney, 2020; Nettelmann et al., 2015); see Figure 1. What's more, even if helium rain is present, it may not lead to stable stratification in the rainout region. Rather, it could be fully convective, or lead to more complicated dynamics. For example, Debras and Chabrier (2019) hypothesize helium rain may cause a double diffusive instability in the vicinity of the upper SSL of our best-fitting model. That is to say, the existence of a stable layer at 0.95 R_J would imply that either our current understanding of the thermodynamics of hydrogen-helium at high pressures would need revision, or that an effect other than the helium gradient may be responsible for the layer. Thus, the mechanism for a stable layer at approximately 0.95 R_J is still an open question.

5. Conclusions

Numerical dynamo models of giant planet interiors provide insights not only into a planet's present day interior structure and dynamics, but also its past formation and evolution. Our new, state-of-the-art simulations featuring SSLs suggest that an upper SSL helps to explain Jupiter's dynamo and winds; the best-fitting model used featured a SSL from 0.90 to 0.95 R_J. In contrast, our models with stably stratified dilute cores provided worse fits to Jupiter's observed field and winds, unless an upper SSL was also included. Our work highlights the ongoing challenges in explaining the planet's origins, and reinforces Jupiter's interdisciplinary nature. As the Juno Mission

continues its extended mission, we hope that future modeling work can benefit additional constraints such as maps of the magnetic field's time-variation, and the geometry of possible wind-sheared field features.

Data Availability Statement

The 3D magnetohydrodynamic (dynamo) modeling code used in this study, MagIC, is available at: https://magic-sph.github.io/.

References

Achterberg, R. K., & Flasar, F. M. (2020). Saturn's atmospheric helium abundance from Cassini composite infrared spectrometer data. *The Planetary Science Journal*, *1*(2), 30. https://doi.org/10.3847/psj/ab9cb6

Alken, P., Thébault, E., Beggan, C. D., Amit, H., Aubert, J., Baerenzung, J., et al. (2021). International geomagnetic reference field: The thirteenth generation. *Earth Planets and Space*, *73*(1), 1–25. https://doi.org/10.1186/s40623-021-01569-z

Braginsky, S. I., & Roberts, P. H. (1995). Equations governing convection in Earth's core and the geodynamo. *Geophysical & Astrophysical Fluid Dynamics*, *79*(1–4), 1–97. https://doi.org/10.1080/03091929508228992

Brygoo, S., Loubeyre, P., Millot, M., Rygg, J., Celliers, P., Eggert, J., et al. (2021). Evidence of hydrogen-helium immiscibility at Jupiter-interior conditions. *Nature*, *593*(7860), 517–521. https://doi.org/10.1038/s41586-021-03516-0

Busse, F. H. (1976). A simple model of convection in the Jovian atmosphere. *Icarus*, *29*(2), 255–260. https://doi.org/10.1016/0019-1035(76)90053-1

Christensen, U. R., Wicht, J., & Dietrich, W. (2020). Mechanisms for limiting the depth of zonal winds in the gas giant planets. *The Astrophysical Journal*, *890*(1), 61. https://doi.org/10.3847/1538-4357/ab698c

Connerney, J., Kotsiaros, S., Oliversen, R., Espley, J., Joergensen, J. L., Joergensen, P., et al. (2018). A new model of Jupiter's magnetic field from Juno's first nine orbits. *Geophysical Research Letters*, *45*(6), 2590–2596. https://doi.org/10.1002/2018gl077312

Connerney, J., Timmins, S., Oliversen, R., Espley, J., Joergensen, J., Kotsiaros, S., et al. (2021). A new model of Jupiter's magnetic field at the completion of Juno's prime mission. *Journal of Geophysical Research: Planets*, *127*(2), e2021JE007055. https://doi.org/10.1029/2021je007055

Conrath, B. J., & Gautier, D. (2000). Saturn helium abundance: A reanalysis of voyager measurements. *Icarus*, *144*(1), 124–134. https://doi.org/10.1006/icar.1999.6265

Conrath, B. J., Gautier, D., Hanel, R. A., & Hornstein, J. S. (1984). The helium abundance of Saturn from voyager measurements. *The Astrophysical Journal*, *282*, 807–815. https://doi.org/10.1086/162267

Debras, F., & Chabrier, G. (2019). New models of Jupiter in the context of Juno and Galileo. *The Astrophysical Journal*, *872*(1), 100. https://doi.org/10.3847/1538-4357/aaff65

Dietrich, W., & Jones, C. (2018). Anelastic spherical dynamos with radially variable electrical conductivity. *Icarus*, *305*, 15–32. https://doi.org/10.1016/j.icarus.2018.01.003

Dietrich, W., & Wicht, J. (2018). Penetrative convection in partly stratified rapidly rotating spherical shells. *Frontiers of Earth Science*, *6*, 189. https://doi.org/10.3389/feart.2018.00189

Duarte, L. D. V., Gastine, T., & Wicht, J. (2013). Anelastic dynamo models with variable electrical conductivity: An application to gas giants. *Physics of the Earth and Planetary Interiors*, *222*, 22–34. https://doi.org/10.1016/j.pepi.2013.06.010

Duarte, L. D. V., Wicht, J., & Gastine, T. (2018). Physical conditions for Jupiter-like dynamo models. *Icarus*, *299*, 206–221. https://doi.org/10.1016/j.icarus.2017.07.016

Fortney, J. J., & Hubbard, W. B. (2003). Phase separation in giant planets: Inhomogeneous evolution of Saturn. *Icarus*, *164*(1), 228–243. https://doi.org/10.1016/s0019-1035(03)00130-1

French, M., Becker, A., Lorenzen, W., Nettelmann, N., Bethkenhagen, M., Wicht, J., & Redmer, R. (2012). Ab initio simulations for material properties along the Jupiter adiabat. *The Astrophysical Journal Supplement Series*, *202*(1), 5. https://doi.org/10.1088/0067-0049/202/1/5

Garaud, P. (2018). Double-diffusive convection at low Prandtl number. *Annual Review of Fluid Mechanics*, *50*(1), 275–298. https://doi.org/10.1146/annurev-fluid-122316-045234

Gastine, T., Aubert, J., & Fournier, A. (2020). Dynamo-based limit to the extent of a stable layer atop Earth's core. *Geophysical Journal International*, *222*(2), 1433–1448. https://doi.org/10.1093/gji/ggaa250

Gastine, T., Heimpel, M., & Wicht, J. (2014). Zonal flow scaling in rapidly-rotating compressible convection. *Physics of the Earth and Planetary Interiors*, *232*, 36–50. https://doi.org/10.1016/j.pepi.2014.03.011

Gastine, T., & Wicht, J. (2012). Effects of compressibility on driving zonal flow in gas giants. *Icarus*, *219*(1), 428–442. https://doi.org/10.1016/j.icarus.2012.03.018

Gastine, T., & Wicht, J. (2021). Stable stratification promotes multiple zonal jets in a turbulent Jovian dynamo model. *Icarus*, *368*, 114514. https://doi.org/10.1016/j.icarus.2021.114514

Gastine, T., Wicht, J., Duarte, L. D. V., Heimpel, M., & Becker, A. (2014). Explaining Jupiter's magnetic field and equatorial jet dynamics. *Geophysical Research Letters*, *41*(15), 5410–5419. https://doi.org/10.1002/2014GL060814

Gilman, P. A., & Glatzmaier, G. A. (1981). Compressible convection in a rotating spherical shell. I-Anelastic equations. II-A linear anelastic model. III-Analytic model for compressible vorticity waves. *The Astrophysical Journal Supplement Series*, *45*, 335–388. https://doi.org/10.1086/190714

Gómez-Pérez, N., Heimpel, M., & Wicht, J. (2010). Effects of a radially varying electrical conductivity on 3D numerical dynamos. *Physics of the Earth and Planetary Interiors*, *181*(1), 42–53. https://doi.org/10.1016/j.pepi.2010.03.006

González-Cataldo, F., Wilson, H. F., & Militzer, B. (2014). Ab initio free energy calculations of the solubility of silica in metallic hydrogen and application to giant planet cores. *The Astrophysical Journal*, *787*(1), 79. https://doi.org/10.1088/0004-637x/787/1/79

Gudkova, T., & Zharkov, V. (1999). Models of Jupiter and Saturn after Galileo mission. *Planetary and Space Science*, *47*(10–11), 1201–1210. https://doi.org/10.1016/s0032-0633(99)00044-6

Guillot, T. (1999). A comparison of the interiors of Jupiter and Saturn. *Planetary and Space Science*, *47*(10–11), 1183–1200. https://doi.org/10.1016/s0032-0633(99)00043-4

Guillot, T., Miguel, Y., Militzer, B., Hubbard, W., Kaspi, Y., Galanti, E., et al. (2018). A suppression of differential rotation in Jupiter's deep interior. *Nature*, *555*(7695), 227–230. https://doi.org/10.1038/nature25775

Heimpel, M., & Gómez Pérez, N. (2011). On the relationship between zonal jets and dynamo action in giant planets. *Geophysical Research Letters*, *38*(14), L14201. https://doi.org/10.1029/2011GL047562

Helled, R., & Morbidelli, A. (2021). Planet formation. In N. Madhusudhan (Ed.), *Exofrontiers; big questions in exoplanetary science*. https://doi.org/10.1088/2514-3433/abfa8fch12

Helled, R., Stevenson, D. J., Lunine, J. I., Bolton, S. J., Nettelmann, N., Atreya, S., et al. (2022). Revelations on Jupiter's formation, evolution and interior: Challenges from Juno results. *Icarus*, *378*, 114937. https://doi.org/10.1016/j.icarus.2022.114937

Hubbard, W. B., & Militzer, B. (2016). A preliminary Jupiter model. *The Astrophysical Journal*, *820*(1), 80. https://doi.org/10.3847/0004-637x/820/1/80

Johansen, A., & Lambrechts, M. (2017). Forming planets via pebble accretion. *Annual Review of Earth and Planetary Sciences*, *45*(1), 359–387. https://doi.org/10.1146/annurev-earth-063016-020226

Jones, C. (2014). A dynamo model of Jupiter's magnetic field. *Icarus*, *241*, 148–159. https://doi.org/10.1016/j.icarus.2014.06.020

Jones, C., Boronski, P., Brun, A., Glatzmaier, G., Gastine, T., Miesch, M., & Wicht, J. (2011). Anelastic convection-driven dynamo benchmarks. *Icarus*, *216*(1), 120–135. https://doi.org/10.1016/j.icarus.2011.08.014

Kaspi, Y., Galanti, E., Hubbard, W., Stevenson, D., Bolton, S., Iess, L., et al. (2018). Jupiter's atmospheric jet streams extend thousands of kilometres deep. *Nature*, *555*(7695), 223–226. https://doi.org/10.1038/nature25793

Koskinen, T., & Guerlet, S. (2018). Atmospheric structure and helium abundance on Saturn from Cassini/UVIS and CIRS observations. *Icarus*, *307*, 161–171. https://doi.org/10.1016/j.icarus.2018.02.020

Lantz, S., & Fan, Y. (1999). Anelastic magnetohydrodynamic equations for modeling solar and stellar convection zones. *The Astrophysical Journal Supplement Series*, *121*(1), 247–264. https://doi.org/10.1086/313187

Leconte, J., & Chabrier, G. (2012). A new vision of giant planet interiors: Impact of double diffusive convection. *Astronomy & Astrophysics*, *540*, A20. https://doi.org/10.1051/0004-6361/201117595

Leconte, J., & Chabrier, G. (2013). Layered convection as the origin of Saturn's luminosity anomaly. *Nature Geoscience*, *6*(5), 347–350. https://doi.org/10.1038/ngeo1791

Liu, S.-F., Hori, Y., Müller, S., Zheng, X., Helled, R., Lin, D., & Isella, A. (2019). The formation of Jupiter's diluted core by a giant impact. *Nature*, *572*(7769), 355–357. https://doi.org/10.1038/s41586-019-1470-2

Lorenzen, W., Holst, B., & Redmer, R. (2011). Metallization in hydrogen-helium mixtures. *Physical Review B*, *84*(23), 235109. https://doi.org/10.1103/physrevb.84.235109

Lowes, F. (1966). Mean-square values on sphere of spherical harmonic vector fields. *Journal of Geophysical Research*, *71*(8), 2179. https://doi.org/10.1029/jz071i008p02179

Mankovich, C. R., & Fortney, J. J. (2020). Evidence for a dichotomy in the interior structures of Jupiter and Saturn from helium phase separation. *The Astrophysical Journal*, *889*(1), 51. https://doi.org/10.3847/1538-4357/ab6210

Mankovich, C. R., & Fuller, J. (2021). A diffuse core in Saturn revealed by ring seismology. *Nature Astronomy*, *5*(11), 1103–1109. https://doi.org/10.1038/s41550-021-01448-3

Miguel, Y., Bazot, M., Guillot, T., Howard, S., Galanti, E., Kaspi, Y., et al. (2022). Jupiter's inhomogeneous envelope. *Astronomy and Astrophysics*, *662*, 1–16. https://doi.org/10.1051/0004-6361/202243207

Miguel, Y., Guillot, T., & Fayon, L. (2016). Jupiter internal structure: The effect of different equations of state. *Astronomy & Astrophysics*, *596*, A114. https://doi.org/10.1051/0004-6361/201629732

Militzer, B., Hubbard, W. B., Wahl, S., Lunine, J. I., Galanti, E., Kaspi, Y., et al. (2022). Juno spacecraft measurements of Jupiter's gravity imply a dilute core. *The Planetary Science Journal*, *3*(8), 185. https://doi.org/10.3847/psj/ac7ec8

Moll, R., Garaud, P., Mankovich, C., & Fortney, J. (2017). Double-diffusive erosion of the core of Jupiter. *The Astrophysical Journal*, *849*(1), 24. https://doi.org/10.3847/1538-4357/aa8d74

Moore, K., Bloxham, J., Connerney, J., Jørgensen, J., & Merayo, J. (2017). The analysis of initial Juno magnetometer data using a sparse magnetic field representation. *Geophysical Research Letters*, *44*(10), 4687–4693. https://doi.org/10.1002/2017gl073133

Moore, K., Cao, H., Bloxham, J., Stevenson, D., Connerney, J., & Bolton, S. (2019). Time variation of Jupiter's internal magnetic field consistent with zonal wind advection. *Nature Astronomy*, *3*(8), 730–735. https://doi.org/10.1038/s41550-019-0772-5

Moore, K., Yadav, R., Kulowski, L., Cao, H., Bloxham, J., Connerney, J., et al. (2018). A complex dynamo inferred from the hemispheric dichotomy of Jupiter's magnetic field. *Nature*, *561*(7721), 76–78. https://doi.org/10.1038/s41586-018-0468-5

Morales, M. A., Hamel, S., Caspersen, K., & Schwegler, E. (2013). Hydrogen-helium demixing from first principles: From diamond anvil cells to planetary interiors. *Physical Review B*, *87*(17), 174105. https://doi.org/10.1103/physrevb.87.174105

Morales, M. A., Schwegler, E., Ceperley, D., Pierleoni, C., Hamel, S., & Caspersen, K. (2009). Phase separation in hydrogen–helium mixtures at mbar pressures. *Proceedings of the National Academy of Sciences of the United States of America*, *106*(5), 1324–1329. https://doi.org/10.1073/pnas.0812581106

Movshovitz, N., Fortney, J. J., Mankovich, C., Thorngren, D., & Helled, R. (2020). Saturn's probable interior: An exploration of Saturn's potential interior density structures. *The Astrophysical Journal*, *891*(2), 109. https://doi.org/10.3847/1538-4357/ab71ff

Müller, S., Helled, R., & Cumming, A. (2020). The challenge of forming a fuzzy core in Jupiter. *Astronomy & Astrophysics*, *638*, A121. https://doi.org/10.1051/0004-6361/201937376

Nettelmann, N., Fortney, J., Moore, K., & Mankovich, C. (2015). An exploration of double diffusive convection in Jupiter as a result of hydrogen–helium phase separation. *Monthly Notices of the Royal Astronomical Society*, *447*(4), 3422–3441. https://doi.org/10.1093/mnras/stu2634

Nettelmann, N., Holst, B., Kietzmann, A., French, M., Redmer, R., & Blaschke, D. (2008). Ab initio equation of state data for hydrogen, helium, and water and the internal structure of Jupiter. *The Astrophysical Journal*, *683*(2), 1217–1228. https://doi.org/10.1086/589806

Nettelmann, N., Movshovitz, N., Ni, D., Fortney, J., Galanti, E., Kaspi, Y., et al. (2021). Theory of figures to the seventh order and the interiors of Jupiter and Saturn. *The Planetary Science Journal*, *2*(6), 241. https://doi.org/10.3847/psj/ac390a

Niemann, H., Atreya, S., Carignan, G., Donahue, T., Haberman, J., Harpold, D., et al. (1998). The composition of the Jovian atmosphere as determined by the Galileo probe mass spectrometer. *Journal of Geophysical Research*, *103*(E10), 22831–22845. https://doi.org/10.1029/98je01050

Pollack, J. B., Hubickyj, O., Bodenheimer, P., Lissauer, J. J., Podolak, M., & Greenzweig, Y. (1996). Formation of the giant planets by concurrent accretion of solids and gas. *Icarus*, *124*(1), 62–85. https://doi.org/10.1006/icar.1996.0190

Schöttler, M., & Redmer, R. (2018). Ab initio calculation of the miscibility diagram for hydrogen-helium mixtures. *Physical Review Letters*, *120*(11), 115703. https://doi.org/10.1103/physrevlett.120.115703

Sharan, S., Langlais, B., Amit, H., Thebault, E., Pinceloup, M., & Verhoeven, O. (2022). The internal structure and dynamics of Jupiter unveiled by a high-resolution magnetic field and secular variation model. *Geophysical Research Letters*, *49*(15), e2022GL098839. https://doi.org/10.1029/2022gl098839

Shibata, S., & Helled, R. (2022). Enrichment of Jupiter's atmosphere by late planetesimal bombardment. *The Astrophysical Journal Letters*, *926*(2), L37. https://doi.org/10.3847/2041-8213/ac54b1

Sromovsky, L., Baines, K., Fry, P., & Momary, T. (2016). Cloud clearing in the wake of Saturn's great storm of 2010–2011 and suggested new constraints on Saturn's He/H_2 ratio. *Icarus*, *276*, 141–162. https://doi.org/10.1016/j.icarus.2016.04.031

Stanley, S. (2010). A dynamo model for axisymmetrizing Saturn's magnetic field. *Geophysical Research Letters*, *37*(5), L05201. https://doi.org/10.1029/2009GL041752

Stanley, S., & Bloxham, J. (2004). Convective-region geometry as the cause of Uranus' and Neptune's unusual magnetic fields. *Nature*, *428*(6979), 151–153. https://doi.org/10.1038/nature02376

Stanley, S., & Bloxham, J. (2006). Numerical dynamo models of Uranus' and Neptune's magnetic fields. *Icarus*, *184*(2), 556–572. https://doi.org/10.1016/j.icarus.2006.05.005

Stevenson, D. (1982). Reducing the non-axisymmetry of a planetary dynamo and and application to Saturn. *Geophysical & Astrophysical Fluid Dynamics*, *21*(1–2), 113–127. https://doi.org/10.1080/03091928208209008

Stevenson, D., & Salpeter, E. (1977). The phase diagram and transport properties for hydrogen-helium fluid planets. *The Astrophysical Journal Supplement Series*, *35*(10), 221–237. https://doi.org/10.1086/190478

Takehiro, S.-I., & Lister, J. R. (2001). Penetration of columnar convection into an outer stably stratified layer in rapidly rotating spherical fluid shells. *Earth and Planetary Science Letters*, *187*(3–4), 357–366. https://doi.org/10.1016/s0012-821x(01)00283-7

Tollefson, J., Wong, M. H., de Pater, I., Simon, A. A., Orton, G. S., Rogers, J. H., et al. (2017). Changes in Jupiter's zonal wind profile preceding and during the Juno mission. *Icarus*, *296*, 163–178. https://doi.org/10.1016/j.icarus.2017.06.007

Vasavada, A. R., & Showman, A. P. (2005). Jovian atmospheric dynamics: An update after Galileo and Cassini. *Reports on Progress in Physics*, *68*(8), 1935–1996. https://doi.org/10.1088/0034-4885/68/8/r06

Wahl, S. M., Hubbard, W. B., Militzer, B., Guillot, T., Miguel, Y., Movshovitz, N., et al. (2017). Comparing Jupiter interior structure models to Juno gravity measurements and the role of a dilute core. *Geophysical Research Letters*, *44*(10), 4649–4659. https://doi.org/10.1002/2017gl073160

Wahl, S. M., Wilson, H. F., & Militzer, B. (2013). Solubility of iron in metallic hydrogen and stability of dense cores in giant planets. *The Astrophysical Journal*, *773*(2), 95. https://doi.org/10.1088/0004-637x/773/2/95

Wilson, H. F., & Militzer, B. (2011). Solubility of water ice in metallic hydrogen: Consequences for core erosion in gas giant planets. *The Astrophysical Journal*, *745*(1), 54. https://doi.org/10.1088/0004-637x/745/1/54

Yadav, R. K., Gastine, T., Christensen, U. R., Wolk, S. J., & Poppenhaeger, K. (2016). Approaching a realistic force balance in geodynamo simulations. *Proceedings of the National Academy of Sciences of the United States of America*, *113*(43), 12065–12070. https://doi.org/10.1073/pnas.1608998113

Yan, C., & Stanley, S. (2021). Recipe for a Saturn-like dynamo. *AGU Advances*, *2*(2), e2020AV000318. https://doi.org/10.1029/2020av000318